processes

MDPI

Article

Study on the Evolution of Mechanical Properties and Acoustic Emission of Medium-Permeability Sandstone under Multi-Level Cyclic Loading Stress Paths

Debin Xia [1,2], Hejuan Liu [1,2], Jianjun Liu [1,2], Yintong Guo [1,2], Mancang Liu [3,*], Xiaosong Qiu [3], Haibo Li [4], Hongying Tan [5] and Jun Lu [6]

1 Institute of Rock and Soil Mechanics, Chinese Academy of Sciences, Wuhan 430071, China; xiadebin21@163.com (D.X.); hjliu@whrsm.ac.cn (H.L.); jjliu@whrsm.ac.cn (J.L.); ytguo@whrsm.ac.cn (Y.G.)
2 State Key Laboratory of Geomechanics and Geotechnical Engineering, Institute of Rock and Soil Mechanics, Chinese Academy of Sciences, Wuhan 430071, China
3 Key Laboratory of Underground Storage of Oil and Gas Engineer of China National Petroleum Corporation, Langfang 065007, China; qiuxiaos69@petrochina.com.cn
4 Research Institute of Petroleum Exploration & Development, PetroChina Company Limited, Beijing 100083, China; lihaibo05@petrochina.com.cn
5 State Key Laboratory of Coal Mine Disaster and Control, Chongqing University, Chongqing 400044, China; tanhongying2021@126.com
6 Institute of Deep Earth Science and Green Energy, College of Civil and Transportation Engineering, Shenzhen University, Shenzhen 518060, China; junlu@szu.edu.cn
* Correspondence: liumc69@petrochina.com.cn

Abstract: Depleted gas reservoirs are important natural gas storage media, thus research on the mechanical properties and damage evolution of reservoir rocks under alternating load conditions has significant practical implications for seal integrity studies. This paper conducted multi-level cyclic loading triaxial compression experiments on medium-porosity medium-permeability sandstone under different confining pressures and used acoustic emission (AE) instruments to detect the AE characteristics during the experiment, analyzing the mechanical characteristics, AE, and damage evolution characteristics. The experimental results show that after cyclic loading, the peak strength of sandstone increased by 14–17%. With the increase in the upper limit stress of cyclic loading, the elastic modulus showed a trend of first increasing and then gradually decreasing. The damage variable of rock samples rose with a rise in the upper limit stress of cyclic loading and confining pressure, and the rock damage was mostly localized at the peak stress. The AE b-value increased generally as confining pressure increased, showing that fractures occurred quicker and more unevenly at lower confining pressures. The distribution of RA-AF values shows that a sudden increase in stress causes the initiation and expansion of cracks in medium-permeability sandstone, and that tensile and shear cracks form continuously during the cyclic loading process, with shear cracks developing more pronounced. This research can provide some theoretical guidance for the long-term stable operation and pressure enhancement expansion of depleted gas reservoir storage facilities.

Keywords: underground gas storage; triaxial compression; mechanical properties; acoustic emission; damage evolution

check for updates

Citation: Xia, D.; Liu, H.; Liu, J.; Guo, Y.; Liu, M.; Qiu, X.; Li, H.; Tan, H.; Lu, J. Study on the Evolution of Mechanical Properties and Acoustic Emission of Medium-Permeability Sandstone under Multi-Level Cyclic Loading Stress Paths. *Processes* **2024**, *12*, 1773. https://doi.org/10.3390/pr12081773

Academic Editors: Carlos Sierra Fernández and Chuanliang Yan

Received: 13 June 2024
Revised: 12 August 2024
Accepted: 19 August 2024
Published: 21 August 2024

1. Introduction

As of 2018, among 662 underground natural gas storage reservoirs in the world, there are 486 depleted reservoir-type storage reservoirs, accounting for 73.4% of the total number, and depleted reservoir-type storage reservoirs are more important natural gas storage space in the world at present [1,2]. Oil and gas reservoirs are relatively well sealed in the previous development stage, but after being converted into gas storage reservoirs, the cyclic high-intensity injection and extraction conditions will produce repeated stress

concentration and relaxation phenomena inside the storage cap rock. This will lead to gradual deterioration of the rock microstructure, affecting its macro-mechanical behavior and long-term stability, and placing the reservoirs at risk of seal failure. Therefore, it is of great significance to study the mechanical characteristics and damage evolution process and features during triaxial compression of rocks under cyclic loading conditions for the safety and stability of gas storage reservoirs.

Researchers have carried out a large number of studies on cyclic loading experiments in rocks, and these research works show that the frequency of cyclic loading, amplitude stress, temperature, permeability, and confining pressure all have a large impact on the mechanical properties and damage deformation of sandstone [3–7]. According to the different experimental control methods, they are mainly divided into two main categories: stress control and strain control [8–17], which are categorized as shown in Figure 1. Depending on the increase of peak-valley strain, it can be categorized into cyclic loading tests in which the peak-valley strain is kept constant (type V) and cyclic loading tests in which the peak-valley strain is gradually increased (type VI) [18]. When strain control is used, there is a possibility that the rock samples may be damaged when a certain strain value is reached, and cyclic loading cannot be performed. Researchers choose different experimental methods according to different purposes, and currently there are more cyclic loading experimental methods using stress control [19–27]. For the first type of experimental method, if it is carried out at stresses below a certain threshold, the rock samples will not be damaged even if the cyclic cycles are greater than 10,000. If under a larger stress state (near the peak stress), the rock is destroyed when the cycle number is very small, and it is difficult to study the change rule of mechanical properties of rock samples during the cycle. For the gas storage reservoir conditions studied in this paper, the fourth type of experimental method is more appropriate. In addition, fewer studies have explored the effect of cyclic loading of multiple stress levels on rock behavior under different confining pressure conditions. This is because in systematic cyclic loading tests, a constant load amplitude has to be achieved in each cycle, and the axial load is difficult to control.

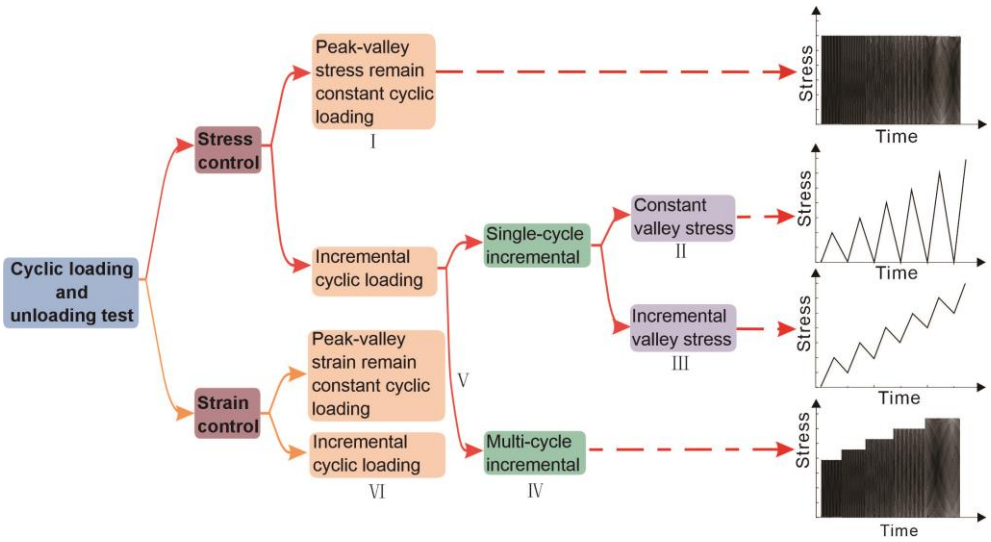

Figure 1. Classification of cyclic loading tests.

During the cyclic loading process, the rock is gradually damaged and deformed until it is destroyed, with the nature of the damage and deformation process being the appearance, expansion, and combination of microcracks [28,29]. During this process, the strain energy contained in the rock is quickly released in the form of transitory elastic waves, resulting in AE [30,31]. As a result, a non-destructive AE detection approach may be employed to investigate the damage and deformation processes of rocks [32]. Tang et al. [33] established the association between the cumulative AE parameters and the degree of rock damage by defining the damage variable as the ratio of the cumulative

number of an AE counts to the entire cumulative number of rocks suffering damage. In order to investigate the internal damage and crack extension of the rock, Zhao et al. [34] employed an AE device to identify the cyclic loading process of Pakistani salt rock in real time. They then methodically examined the characteristics, such as AE counts, peak frequency, and amplitude. Li et al. [35] conducted uniaxial and triaxial creep-fatigue experiments on salt rock. Using AE detection equipment, they identified AE signals during the experiment, and they then used the theory of continuum damage mechanics to calculate the salt rock's damage based on the correlation between the AE counts and the damage variables. Thanks to these researches, it is now possible to continually monitor the damage deformation during cyclic loading using AE, a non-destructive monitoring method.

The cyclic loading process is also a process in which the macroscopic mechanics of the rock will gradually deteriorate, and this process is also a process of damage development accompanied by energy dissipation [36], so a scalar damage that can comprehensively respond to the anisotropy of the rock can be established from the energy point of view. Li et al. [37] established a damage model for dolomite that takes into account the initial damage of the rock based on the principle of energy dissipation and introduced the equivalent modulus concept. And, based on the experimental data, the results were validated, demonstrating that the destruction and damage of the rock samples were strongly connected to energy dissipation, and that the damage model could properly compute the rock's damage in uniaxial compression tests. Gao and Feng [38] conducted true triaxial cyclic loading experiments on intact and joint-containing marble samples and quantified the damage process of the rock by adopting the dissipated energy and irreversible strain as the damage variables. The results showed that the damage variables based on irreversible strain and dissipated energy were closely correlated, and the fitted parameters had intuitive physical significance and specific relationships with the intermediate and minimum principal stresses as well as the joint inclination angle. Chen et al. [39] performed uniaxial compression tests on six different kinds of rocks to investigate the damage development mechanism of the rocks from an energy conversion perspective. Damage coefficients derived from dissipated energy have been presented to quantify the damage status of rocks, introducing a novel way for quantitative assessment of rock damage. The dissipation energy may be utilized to study the damage evolution process in rocks.

In this paper, starting from the operating conditions of depleted gas storage reservoirs, the cyclic loading and unloading experiments of multiple stress levels under four different peripheral pressure conditions (constant stress lower line, stress upper line gradually increasing) were carried out with mesoporous mesoturbulent sandstone as the research object. Damage to the rock samples under different peripheral pressure conditions was quantitatively characterized using two quantitative damage characterization methods of acoustic emission event number and dissipation energy at the same time, which can avoid necessitating the use of single methods. This can avoid the defect of using a single method, which is insufficiently persuasive. The results of this research can provide theoretical guidance for the long and stable operation of underground natural gas storage reservoirs, and the pressure increase and capacity expansion.

2. Experiment Methods and Materials

2.1. Experimental Schemes Design

During the operation of the reservoir, natural gas is injected into the reservoir during the low gas consumption period, and the pore pressure of the reservoir rock is the highest at the end of the injection period; the natural gas in the reservoir is extracted during the peak gas consumption period, and the pore pressure of the reservoir rock is the lowest at the end of the extraction period. In this way, a cyclic injection and extraction pattern is formed, and the reservoir rocks are subjected to cyclic stresses in this operation pattern. In order to study the damage evolution of the reservoir rock under such working conditions, a common sandstone in the reservoir was used for the cyclic loading experiments and an AE device was used to monitor the AE response of the rock during the experimental

process. According to the fact that the burial depth of most gas storage reservoirs in China is concentrated in the range of 2500~3500 m, and most of their working pressures are in the range of 10~40 MPa [2], four different confining pressures are set up, which are 10 MPa, 20 MPa, 30 MPa, and 40 MPa. In order to obtain the critical axial stresses under the four confining pressures, the first step is to carry out proposed triaxial compression experiments. In each kind of confining pressure condition, there are five stress levels, $0.6\sigma_c$, $0.7\sigma_c$, $0.8\sigma_c$, $0.9\sigma_c$, $1.0\sigma_c$, respectively, and 40 cycles are cycled in each stress level condition.

2.2. Medium-Permeability Sandstone Samples

Sandstone has a mean porosity of 17.1% and a mean permeability of 63.9 mD, classified as mesoporous and medium permeability sandstones. We used XRD experiments to analyze the mineral makeup in the rock samples, and the experimental findings revealed that the main composition of the sample is Albite with 60.69%, microcline with 16.45%, quartz with 16.01%, calcite with 3.29%, chlorite with 2.02%, and illite with 1.55%, as shown in Figure 2. The sample information when conventional triaxial compression was performed is shown in Table 1, and the sample information when triaxial cyclic loading was performed is shown in Table 2.

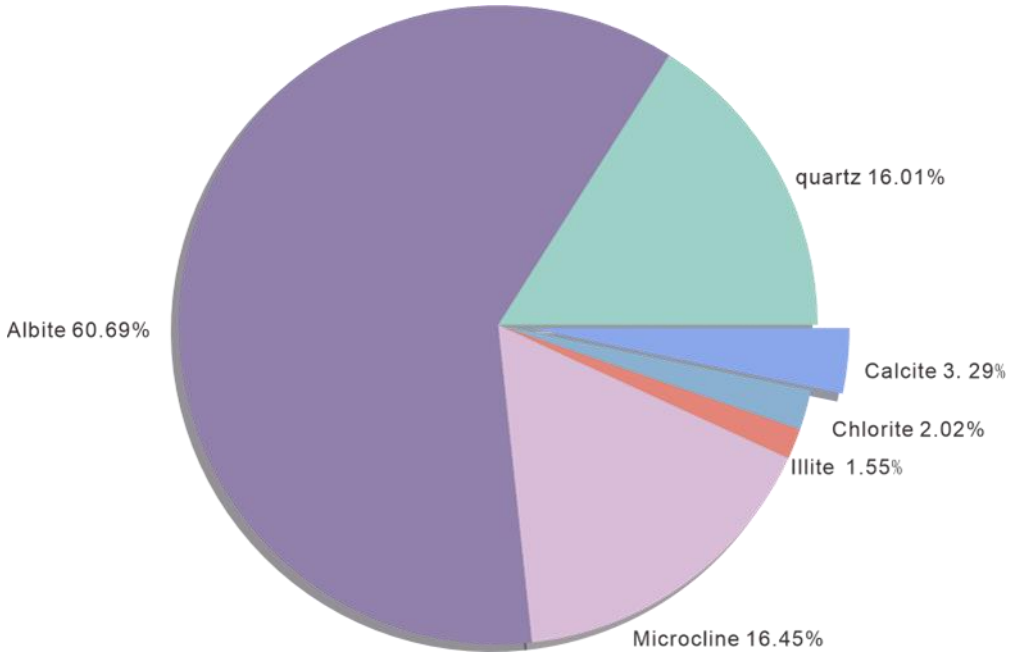

Figure 2. Mineralogical composition of sandstone samples.

2.3. Experimental Equipment and Procedures

This experiment employed an electro-hydraulic servo-controlled rock mechanics testing equipment, which includes a control system, an oil source, a loading structure, a restraining force system, and several test equipment and monitors. The experimental equipment and rock samples, as well as the fixation method is shown in Figure 3:

Because the AE instrument and strain gauge used in this test are two independent systems, to allow the two systems to effectively synchronize the collection of test data to meet the test requirements, the experimental procedure should be conducted as shown in Figure 4:

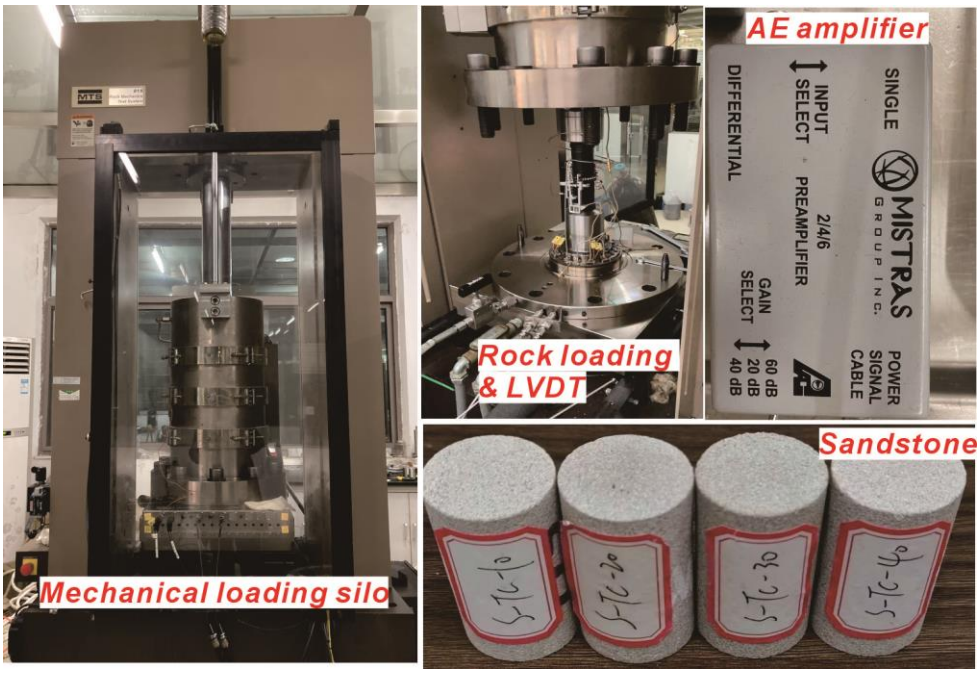

Figure 3. MTS815.04 experimental system with sandstone samples.

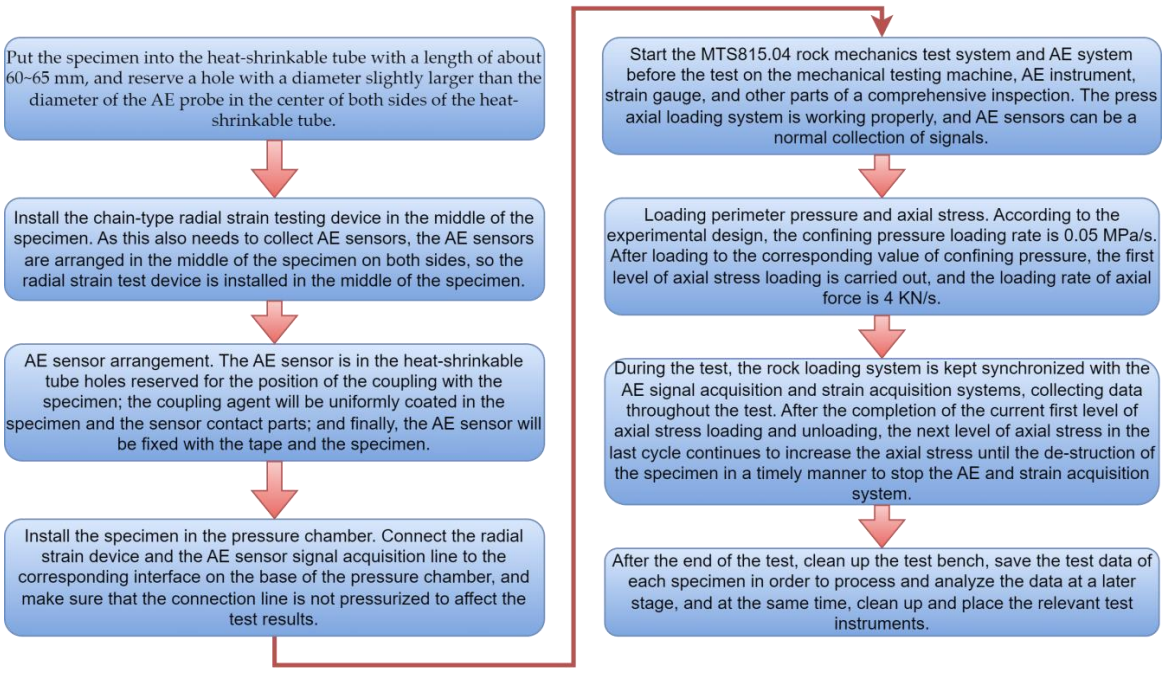

Figure 4. Flowchart of experimental steps.

Table 1. Uniaxial compression rock sample parameters.

Specimen NO.	Confining Pressures (MPa)	Height (mm)	Diameter (mm)
S-U-2	0	51.55	25.08
S-1	10	51.82	25.15
S-2	20	50.01	24.82
S-4	40	50.30	24.92

Table 2. Multilevel cycle loading and unloading experiment sample information.

Specimen NO.	Diameter (mm)	Height (mm)	Confining Pressure (MPa)	Peak Stress (MPa)	Axial Pressure	Number of Cycles
S-TC-10	25.11	50.21	10	117	10 MPa~0.6 σ_c 10 MPa~0.7 σ_c 10 MPa~0.8 σ_c 10 MPa~0.9 σ_c 10 MPa~1.0 σ_c	40
S-TC-20	24.86	50.03	20	143	10 MPa~0.6 σ_c 10 MPa~0.7 σ_c 10 MPa~0.8 σ_c 10 MPa~0.9 σ_c 10 MPa~1.0 σ_c	40
S-TC-30	25.21	50.08	30	164	10 MPa~0.6 σ_c 10 MPa~0.7 σ_c 10 MPa~0.8 σ_c 10 MPa~0.9 σ_c 10 MPa~1.0 σ_c	40
S-TC-40	24.88	49.89	40	186	10 MPa~0.6 σ_c 10 MPa~0.7 σ_c 10 MPa~0.8 σ_c 10 MPa~0.9 σ_c 10 MPa~1.0 σ_c	40

3. Results of the Experiment

3.1. Triaxial Compressive Stress–Strain Curve

The whole stress–strain graph of rock in a typical triaxial compression process is commonly shown in Figure 5, primarily containing the undamaged zone pre the top and the damaged region post the top, and then separated into four parts [22]: the compression stage (OA), in which the primary pores and crack of the rock are compressed, and the specimen's elastic modulus steadily increases, and the stress–strain curve exhibits an upward sloping form, and the presence of the particular OA section in the traditional triaxial compression curve, as well as the amount of it, is determined by the nature of the specimen and the magnitude of the confining pressure during the test. The linear elasticity stage (AB) of the stress–strain graph is essentially linear, demonstrating the nature of linear elasticity, so this stage can be used in the elasticity parameters of the calculations. In the plastic hardening period (BC), the path of stress–strain gradually becomes concave, the ability to resist deformation gradually reduce, start to produce irreversible deformation, the B point began to appear the volume expansion, after which the damage accumulation accelerated. Strain softening stage (CD), for the destruction of the post-destructive zone, the stress reaches the ultimate strength of the specimen damage occurs after the destruction of the destruction is still a part of the load-bearing capacity, but the damage is sharply increased. Among the above four stages, the BC stage is the focus of engineering feasibility analysis, design, operation, maintenance, and monitoring.

From Figure 6, the pre-peak stage of the stress–strain curve has good elastic properties, while the peak point and the strain softening stage can only be maintained for a very short time, showing the characteristics of brittle damage. The proportions of strains in its compressive stage are 23.9%, 17.0%, 15.4% and 10.9%, respectively, and the proportion of strains in the compressive stage gradually decreases; the proportions of strains in the linear elastic stage are 19.3%, 13.0%, 14.7% and 17.3%, respectively, and the proportion of strains in the linear elastic stage gradually increases. With the increase in confining pressure, the peak strength gradually increases, the brittleness decreases, and the plasticity enhances the trend. This phenomenon can be attributed to the effect of the confining pressure on the internal structure of the sandstone. First of all, the increase in the confining pressure can significantly enhance the friction between sandstone particles, which makes it more difficult for the sandstone to be displaced or deformed under stress and increases the shear

strength and compressive strength of the sandstone. In addition, the increase in confining pressure also helps the closure of microcracks inside the sandstone, reducing the damage points inside the sandstone, thus reducing its overall brittleness. This closure process makes the sandstone tougher when subjected to forces, as the reduction in cracks means that the sandstone is less likely to fracture under the same external force.

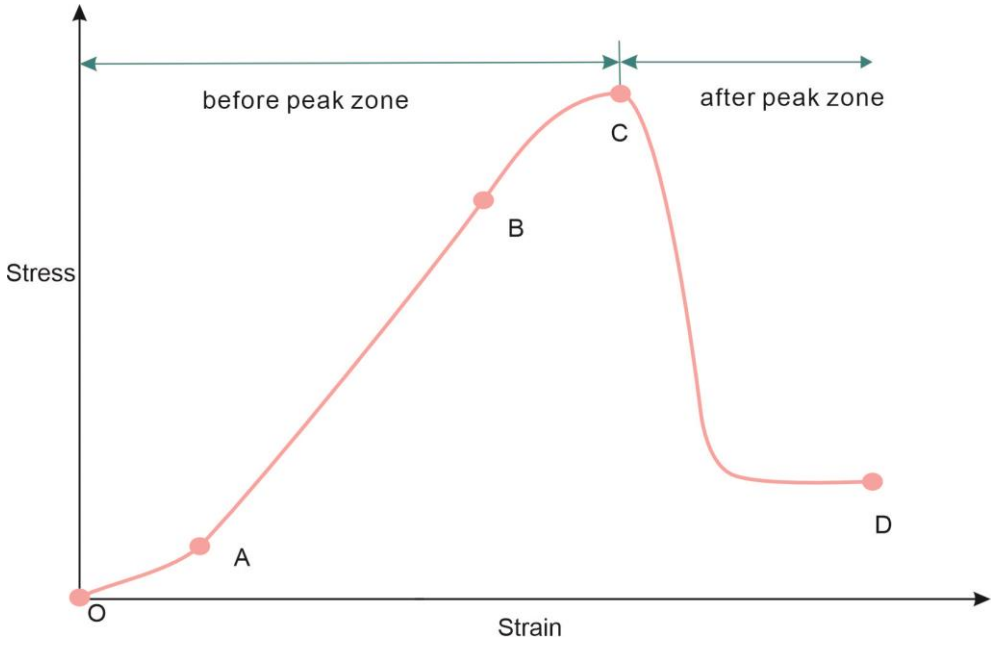

Figure 5. Triaxial compressive stress–strain curves of conventional rock samples.

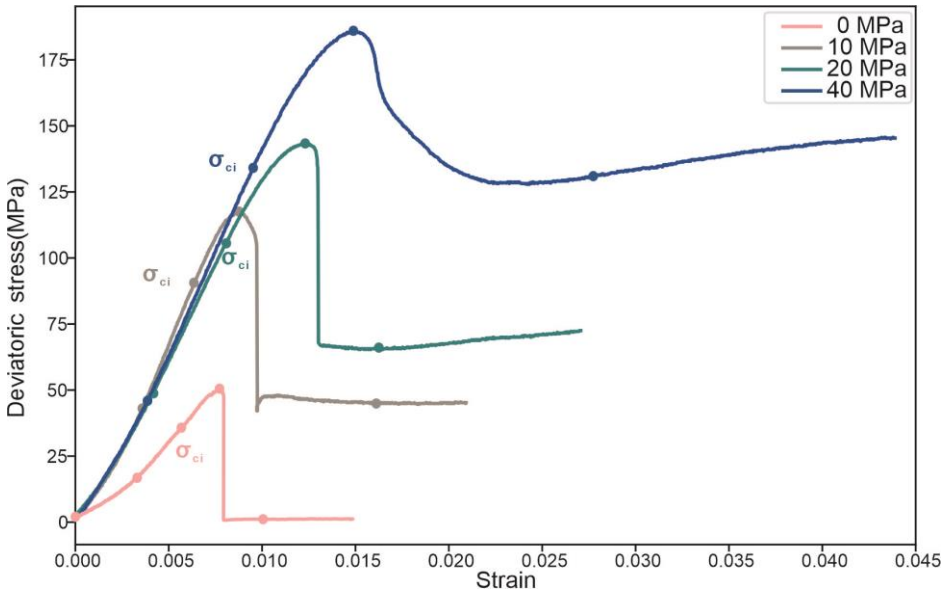

Figure 6. Triaxial compressive stress–strain curves of sandstone at confining pressure 10 MPa, 20 MPa, 30 MPa, and 40 MPa, respectively.

By analyzing the stress–strain curves of the medium permeability sandstone under four confining pressures, its mechanical parameters can be obtained, as shown in Table 3.

Table 3. Mechanical parameters of triaxial compression.

Specimen NO.	Confining Pressure (MPa)	Peak Stress (MPa)	Damage Stress Threshold (MPa)	Elastic Modulus (MPa)	Poisson's Ratio
S-U-2	0	51.12	42.53499	7894	0.16
S-1	10	117.66	91.96987	17,302	0.15
S-2	20	143.30	106.37346	14,843	0.17
S-4	40	186.00	138.99171	15,976	0.15

According to the triaxial compression mechanical parameters of Table 3, the peak stress and damage stress threshold can be fitted and analyzed, as shown in Figure 7. The peak stress and damage stress threshold show a good linear correlation with the confining pressure, and it can be calculated that when the confining pressure is 30 MPa, the peak stress is 164 MPa and the damage stress threshold is 123 MPa.

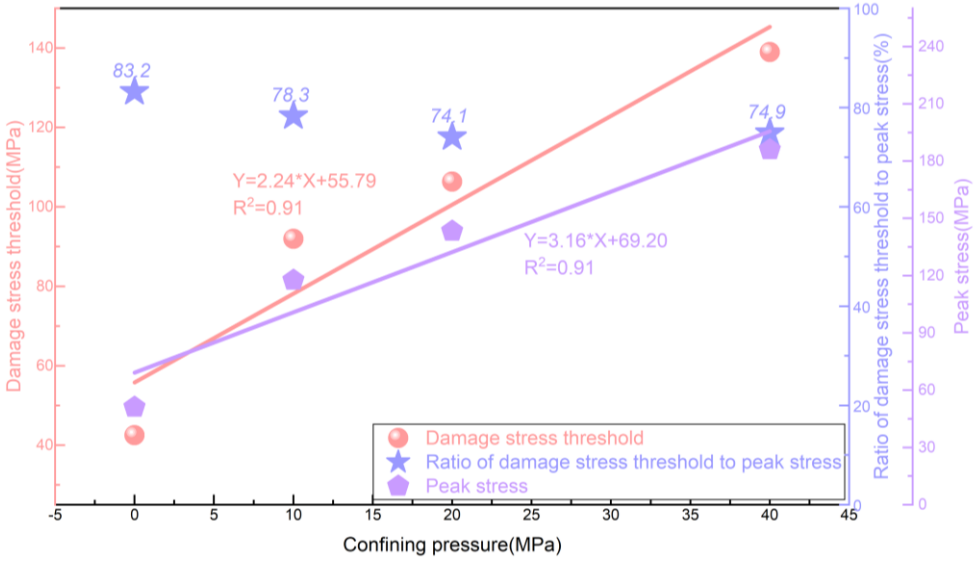

Figure 7. Damage stress threshold and its ratio to peak stress.

3.2. Stress-Strain Curve in Cyclic Loading–Unloading Triaxial Compression

Based on the experimentally measured data, the stress–strain curves were plotted as shown in Figures 8–11:

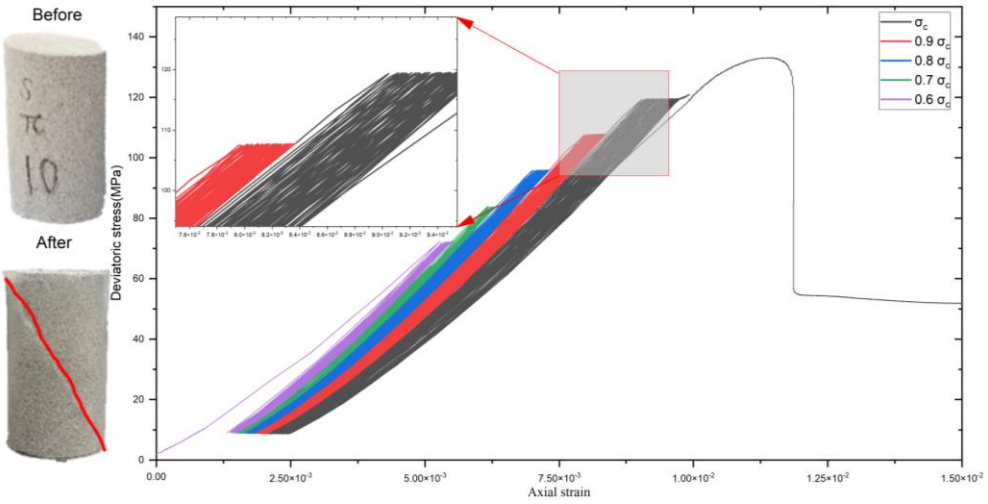

Figure 8. Stress–strain curves at confining pressure of 10 MPa.

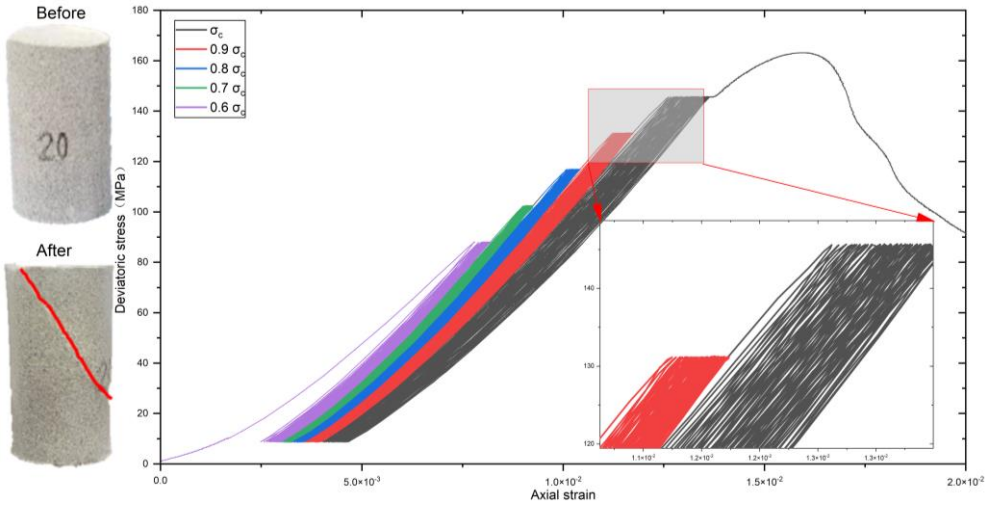

Figure 9. Stress–strain curves at confining pressure of 20 MPa.

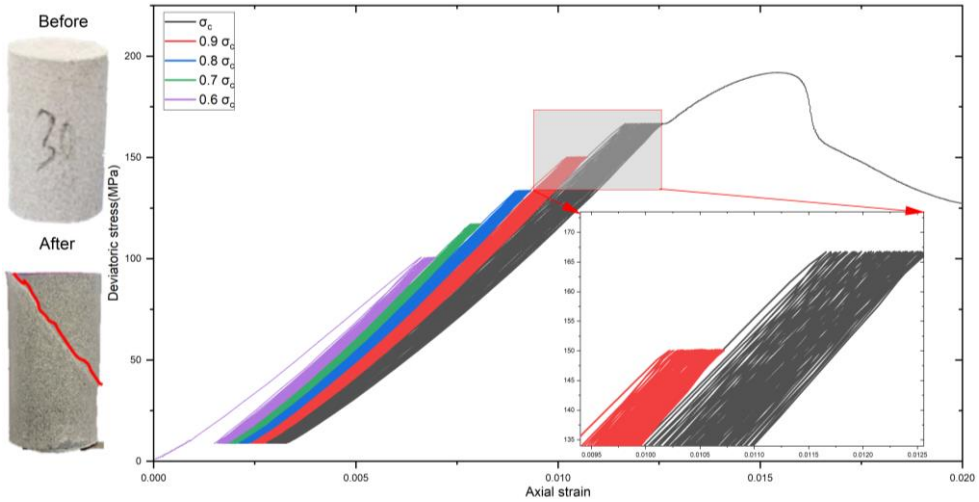

Figure 10. Stress–strain curves at confining pressure of 30 MPa.

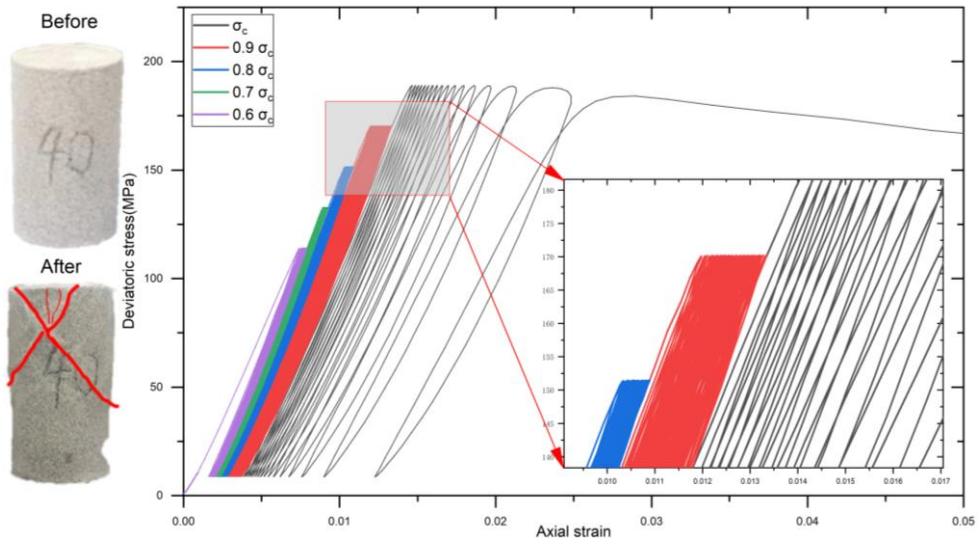

Figure 11. Stress–strain curves at confining pressure of 40 MPa.

From Figures 8–11, it can be observed that the stress–strain curves do not overlap but form hysteresis curves, which is due to the plastic deformation of the rock after cyclic loading experiments. The stress–strain curves under four confining pressure, the hysteresis curves of each stress level are gradually dense with the increase of the number of cycles, which indicates that at the beginning of the cycle due to the instantaneous increase in the applied stress and large plastic deformation, the internal crystals of the rock friction with each other to generate heat and microcracks to expand, which absorbs a greater amount of plastic strain energy, and then gradually stabilized; the area of plastic hysteresis loops is larger at high stress levels, which indicates that the higher stress level of the larger area of plastic hysteresis rings at high stress levels indicates that higher stress levels increase the plastic strain energy of the rock samples, resulting in greater plastic deformation. After five axial stress-level loading experiments at 10 MPa, 20 MPa, and 30 MPa confining pressure conditions, the rock samples experienced large cracks that traversed the entire rock sample. In addition, the peak axial stresses increased by 14–17% compared to the results of the conventional triaxial compression experiments, indicating that undergoing the cyclic loading increased the sandstone's ability to resist deformation and produce hardening phenomena. The experimental results show different characteristics when the peripheral pressure is 40 MPa. In the alternating experiments carried out at this enclosure pressure, several large cracks appeared in the upper part of the rock samples, and the development of these cracks was closely related to the changes in the axial peak stress. Significant damage to the rock samples occurred when the 25^{th} cycle of the fifth stress level was performed. This phenomenon suggests that the strength and stability of the rock is more affected at higher peripheral pressures and the damage pattern of the rock changes.

4. Discussion

4.1. Mechanical Parameters Analysis in Cyclic Loading–Unloading Tests

Figure 12 shows the elastic modulus versus time curves during cyclic loading, from which the elastic modulus of sandstone increases with the increase of the confining pressure. The elastic modulus changes trend of loading and unloading under the four confining pressures is similar, in the low axial stress level, the loading and unloading elastic modulus of sandstone increases with the increase of the number of cyclic cycles. This is due to the initial pore cracks in the rock samples were gradually compacted, the degree of consolidation between the particles and clay minerals in the rock increased, resulting in an increase in the friction between the crystals, the deformation caused by cyclic loading and unloading on the rock samples is smaller, the strengthening effect is greater than the destructive effect, so that the modulus of elasticity of the specimens increased. The greater the confining pressure, making the rock interior denser, the connection between particles is strengthened, slowing down the generation and development of the micro-defects in the rock interior, reducing the damage extension, and the damage expansion. The larger the confining pressure, the denser the rock, the stronger the connection between the particles, the slower the development of micro-defects in the rock, and the lower the damage extension, which makes the larger the confining pressure, the larger the modulus of elasticity under the same axial stress level. At high stress levels, the modulus of elasticity decreases in a stepwise manner with the increase of stress level and the number of cycles. This is due to the fact that the rising stress level and the increasing number of cycles gradually generate new cracks and pores inside the rock samples, which leads to the stronger damage effect than the strengthening effect, and the modulus of elasticity decreases gradually in this stage.

It is noteworthy that the elastic modulus in the unloading stage is larger than that in the loading stage under the same confining pressure and axial stress level conditions. This phenomenon is related to the internal stress state and microstructural changes of the rock under different loading conditions, where the rock undergoes plastic deformation during loading, the internal structure undergoes micro-damage and alteration, and the contact area between the particles is larger, which leads to a relatively low elastic modulus of the rock in the loading stage. However, during the unloading stage, some of the damage may

be repaired, some of the internal microstructures of the rock are rearranged, and the contact area between the particles is relatively reduced, leading to a slight increase in the modulus of elasticity of the rock during the unloading stage.

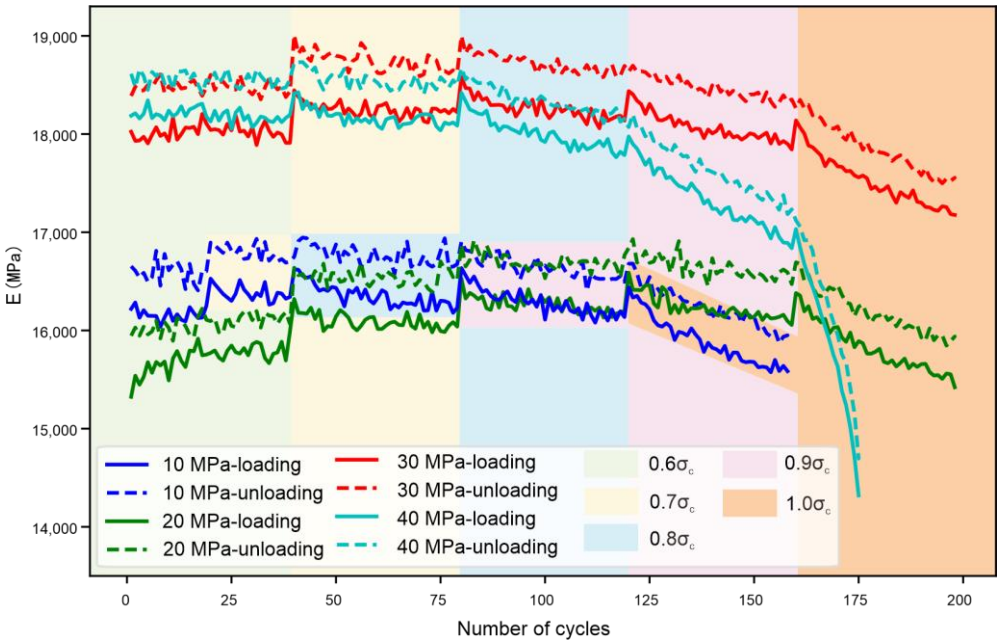

Figure 12. Elastic modulus change curve during cycling test.

4.2. Energy Evolution Analysis in Cyclic Loading–Unloading Tests

Rock is a kind of natural geological body which contains many microcracks and holes internally, under the action of external load, the generation, expansion, penetration of micro-cracks interacting with each other and linking is the essential reason leading to the deterioration of the mechanical properties of rock materials. The key to studying rock damage from the viewpoint of energy is to accurately calculate the energy change of rock at each stage. According to the principle of conservation of energy, the total work done by the test system on the rock sample compression during the loading of the specimen can be obtained by integrating the load-displacement curves measured by the test machine [40], which is calculated as follows:

$$W = \int_L FdL = E_s + E_b + E_r \quad (1)$$

where W is the total work done by the external load; F is the load; L is the deformation of the specimen; E_s is the elastic energy storage of the test system; E_r is the energy absorbed by the test specimen; and E_b is the energy dissipated by the various damping of the test system.

During loading, E_b is very small, so it is not considered in the calculation. As for the elastic energy storage of the test system in the Equation (1), according to the results of literature [40], the larger the MTS stiffness is, the smaller its elastic energy storage E_s is. In this test, the MTS stiffness is much larger than the rock stiffness, and the deformation of the press is negligible, so it can be considered that the elastic energy stored in the test system E_s is 0, and then Equation (1) can be simplified to Equation (2).

$$W = E_r \quad (2)$$

The energy absorbed by the rock can be divided into two parts, one part is dissipated energy, and the other part is elastic strain energy, then Equation (2) can be transformed into Equation (3), and E_r is the total strain energy. The dissipated energy includes the energy absorbed by the rock damage and the plastic deformation energy of the rock. In a loading

and unloading cycle, the rock will release all the elastic strain energy stored inside during the unloading process.

$$W = E_r = U^d + U^e \tag{3}$$

where U^d is the dissipated energy of the rock during loading and unloading; U^e is the elastic strain energy of the rock during loading and unloading.

The calculation of dissipated energy and elastic strain energy can be obtained according to the loading and unloading cyclic stress-axial strain curves, respectively, on the loading and unloading stress–strain curve integral to obtain the area, then the loading stress–strain curve area for the press on the specimen to do the total work of the total strain energy, and unloading stress–strain curve area of the elastic strain energy the difference between the two is the dissipation of energy for the dissipated energy and the elastic strain energy For the calculation of dissipation energy and elastic strain energy, the schematic diagram is shown in Figure 13. It should be noted that, except for the first loading starting point of 0, the starting point of loading and the end point of unloading of the other levels are not 0, so the calculation of the area should be considered. The stress–strain curves in the loading and unloading process under the four confining pressure conditions were obtained according to the method, and the change curves of dissipated energy, elastic deformation energy, input energy and cumulative dissipated energy in the cyclic process were obtained as shown in Figure 14:

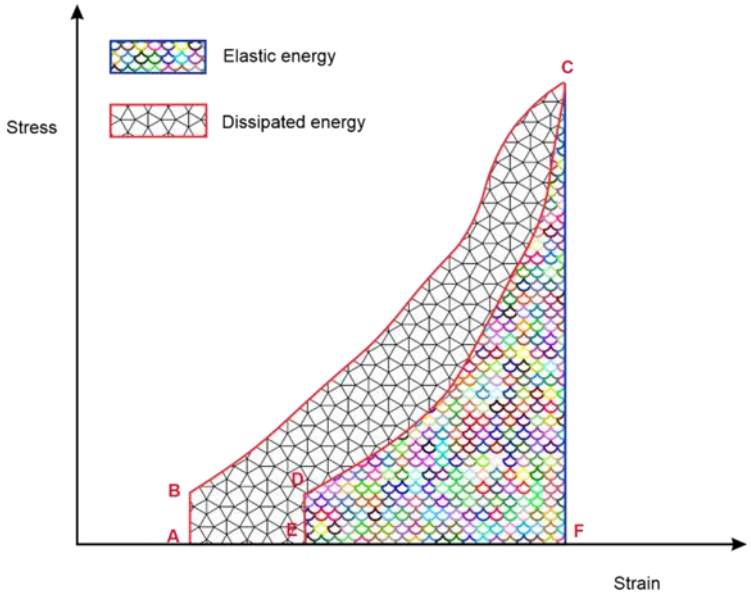

Figure 13. Schematic design for dissipated and elastic strain energy calculation.

In this study, we stipulate that the input of energy is positive while the output of energy is negative. From Figure 14, it is observed that the trends of the curves under the four confining pressure conditions are similar, with both the input and dissipation energies showing a stepwise growth pattern as the axial stress level increases, whereas the elastic deformation energy shows a stepwise decreasing trend. This phenomenon reflects the characteristics of energy conversion and dissipation in sandstone under stress. At the stage of lower axial bias stress level, the input energy, dissipation energy and elastic deformation energy all increase with the increase of stress, but these energy parameters gradually tend to a stable state as the stress level continues to rise. This is due to the adjustment of the microstructure of the sandstone under the initial stress, resulting in changes in the absorption and release of energy. When the axial bias stress reaches the level of $0.9\sigma_c$, the rate of increase of input energy, dissipation energy and elastic deformation energy increases significantly. This indicates that at higher stress levels, more significant changes in the internal structure of the sandstone occur, leading to an increase in the efficiency of

energy absorption and dissipation. In addition, at the same axial stress stage, the input energy, dissipation energy and elastic deformation energy show an increasing trend with the increase of the enclosing pressure. This phenomenon may be related to the increase of internal density and microfracture closure in sandstone due to the peripheral pressure. The increase in confining pressure improved the contact and bonding state between particles within the sandstone, thus affecting the mode of energy transfer and dissipation.

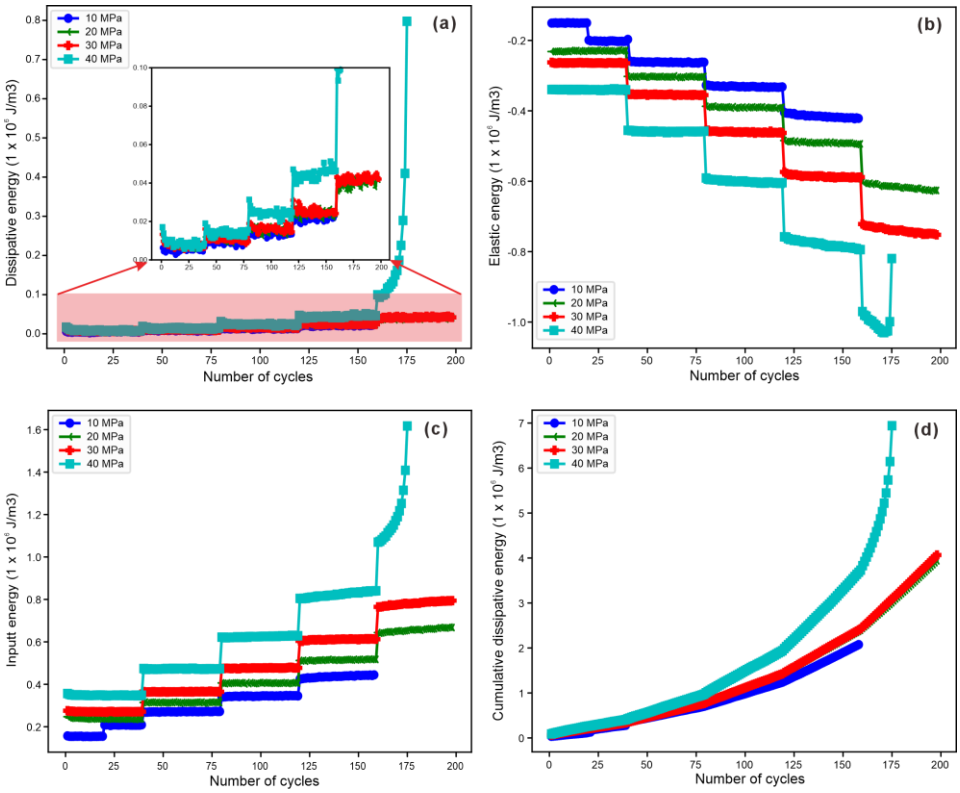

Figure 14. Energy change curves during cycling. (**a**) dissipation energy versus number of cycles, (**b**) elastic energy versus number of cycles, (**c**) input energy versus number of cycles, (**d**) Cumulative energy versus number of cycles.

The deterioration process of rock properties can be described by a continuous internal variable, the damage variable. Dissipation energy is an important parameter for evaluating rock damage, which has a good correlation with the progressive development of rock damage, and defining the damage variable from the perspective of energy dissipation can provide a more comprehensive response to rock damage. Currently, the following formula is used in establishing the rock damage characterization method with dissipated strain energy as the damage variable:

$$D(i) = \frac{U^d(i)}{U^d} \tag{4}$$

where i is the cyclic loading number; $D(i)$ is the damage variable at the i cyclic loading; $U^d(i)$ is the dissipation energy at the i cyclic loading; U^d is the cumulative dissipated energy after rock damage.

From the above equation, it is obvious that when the specimen is not loaded or in the elastic stage, the rock damage and the cumulative damage variable D are both 0. When the damage threshold is exceeded, the rock starts to show damage, considering the damage of

the rock is increasing during the unloading and loading process, so the cumulative damage variable D of the rock at the end of i cyclic loading can be expressed as Equation (5):

$$D = \sum_{1}^{i} D(i) = \frac{\sum_{i}^{i} U^d(i)}{U^d} \quad (5)$$

From the Equation (5), the cumulative damage of the rock after the end of the last cyclic loading is 1, and this calculation method is appropriate for the value of the damage variable in this paper. According to the Formulas (4) and (5) and the previous calculation of the rock specimen energy results, so that we can derive the results of the specimen damage variable and cumulative damage variable in Table 4:

Table 4. Damage variables and cumulative damage variables for different stress levels based on dissipated energy.

Stress Level	10 MPa		20 MPa		30 MPa		40 MPa	
	$D(i)$	$\sum D(i)$	$D(i)$	$\sum D(i)$	$D(i)$	$\sum D(i)$	$D(i)$	$\sum D(i)$
$0.6\sigma_c$	0.0440	0.0440	0.0742	0.0742	0.0703	0.07034	0.0488	0.0488
$0.7\sigma_c$	0.0628	0.1068	0.1160	0.1902	0.1073	0.1776	0.0821	0.1310
$0.8\sigma_c$	0.1747	0.2815	0.1613	0.3515	0.1631	0.3407	0.1418	0.2728
$0.9\sigma_c$	0.2834	0.5649	0.2504	0.6019	0.2514	0.5921	0.2604	0.5332
$1.0\sigma_c$	0.4351	1	0.3981	1	0.4079	1	0.4668	1

Based on the results of damage variables and cumulative damage variables calculated in Table 4, the evolution curves of damage variables and cumulative damage variables are plotted in Figure 15.

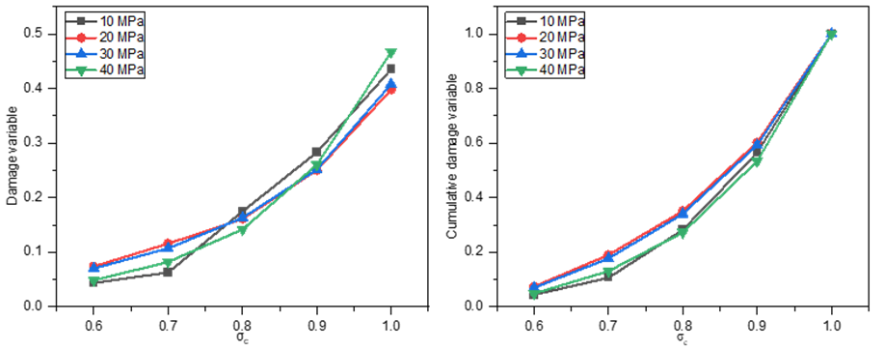

(**a**) (**b**)

Figure 15. Damage variable curves derived from the characterization of dissipated energy. (**a**) damage variable versus stress level, (**b**) cumulative damage variable versus stress level.

From Figure 15, the damage variables and cumulative damage variables under different confining pressures have similar trends, and both increase with the increase of stress level. In the low stress state, the rock damage variable is small, and the growth rate of cumulative damage variable is slow, thereafter, with the increase of stress level, the cracks develop stably, and obvious damage occurs, and the growth rate of cumulative damage variable appears to increase. When the loading cycle enters the high stress level, the cracks develop non-stably, the rock damage variable increases significantly, and the growth rate of the cumulative damage variable increases again. The relationship curve between the cumulative damage variable and the stress level shows an "upward concave" state, and the increase of the rock damage variable is very obvious under the last level of loading, with an average of about 0.43, which indicates that, based on the dissipated energy method to characterize the rock damage, the rock damage is mainly in the stage of unsteady develop-

ment of cracks, the rock damage is mainly concentrated in the stage of the approaching stress peak.

4.3. AE Count Characteristic Analysis in Cyclic Loading–Unloading Tests

There is a very close relationship between rock damage and AE, and the AE activity represents the degree of rock microdamage. Therefore, the AE counts can be used to analyse the deformation, damage and destruction evolution of rocks. The experimentally measured AE event counts, stress data and time are plotted in a graph as shown in Figure 16:

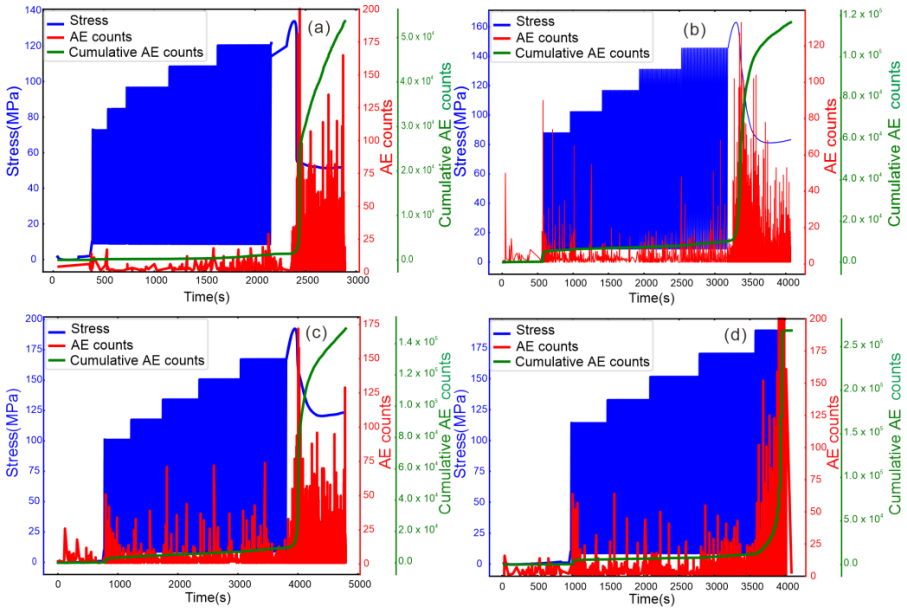

Figure 16. Number of AE and cumulative AE counts during cycling test. (**a**) 10 MPa confining pressure, (**b**) 20 MPa confining pressure, (**c**) 30 MPa confining pressure, (**d**) 40 MPa confining pressure.

As can be seen from Figure 16, some jump points with larger number of AE counts (values between 25 and 100) can be observed in each axial stress level. The number of these jumping points increases gradually with the increase of the confining pressure, and this phenomenon suggests that some tiny cracks may have been generated inside the rock during the cyclic loading experiments. In the three groups of 10 MPa, 20 MPa, and 30 MPa experiments, when the axial stress reaches the vicinity of the peak value, the number of AE counts with multiple values greater than 100 can be observed. This suggests that larger macroscopic cracks have appeared in the rock and eventually penetrated leading to the rupture of the rock. At a confining pressure of 40 MPa, multiple AE counts with values greater than 100 are observed at the last stress level, again indicating large cracks and subsequent rock damage. In conjunction with the form of rock damage, it can be seen that the value and intensity of the number of AE counts are closely related to the form of rock damage.

Based on the principle of statistics and the special properties of rocks, it can be assumed that a certain cross-section of a rock consists of a large number of microelements with varying degrees of defects, and it is believed that these microelements have different strengths, and the strengths of the microelements obey a statistical distribution. When an external load is applied to a rock specimen, the strain is assumed to be uniformly distributed, and the strain of the specimen increases with the increase of the external load or the passage of time, and when the strain exceeds the strength of some of the microelements, these microelements exceeding the strength will be destroyed after another. Therefore, the area of the rock specimen cross-section showing damage can be expressed as [41]:

$$S = S_m \cdot \int_0^{\varepsilon} \varphi(x)dx \tag{6}$$

where S_m is the cross-sectional area of the material in its undamaged state; $\varphi(x)$ is the statistical distribution of the strength of the microelement.

Therefore, the rock damage parameter D can be given by the following equation:

$$D = S/S_m = \int_0^{\varepsilon} \varphi(x)dx \tag{7}$$

Assuming that AE counts produced per unit area of damaged microelements is n, AE counts ΔN that will be produced by the damaged area ΔS can be expressed as:

$$\Delta N = n \cdot \Delta S = N_m \frac{\Delta S}{S_m} \tag{8}$$

where N_m is the cumulative number of AE impacts when the damage area is S_m.

When the strain increment of the specimen is $\Delta\varepsilon$, the corresponding damage area ΔS of the specimen can be calculated by the following formula:

$$\Delta S = S_m \cdot \varphi(\varepsilon) \cdot \Delta\varepsilon \tag{9}$$

When the strain produced by the specimen is increased to ε, the ratio of the cumulative AE counts to the cumulative AE counts at full damage can be obtained as follows:

$$N/N_m = \int_0^{\varepsilon} \varphi(x)dx \tag{10}$$

Combining Equations (7) and (10) above yields an important equation for the relationship between the damage variable D and the number of AE counts N:

$$D = N/N_m \tag{11}$$

From Equation (11), it can be seen that the damage variables of the rock are consistent with the AE of the rock, and for the cyclic loading experiments, the following equations are used for the calculation of the damage variables in each cyclic phase:

$$D_i = \sum_1^i N_i/N_m \tag{12}$$

where $D(i)$ is the damage variable at the i cyclic loading; N_i is the AE counts at the i cyclic loading.

According to the experimental results, the collected AE data were organized, and the cumulative AE counts obtained for each specimen during the loading stages are shown in Table 5.

Table 5. Damage variables and cumulative damage variables for different stress levels based on AE counts.

Stress Level	10 MPa		20 MPa		30 MPa		40 MPa	
	$D(i)$	$\sum D(i)$	$D(i)$	$\sum D(i)$	$D(i)$	$\sum D(i)$	$D(i)$	$\sum D(i)$
$0.6\sigma_c$	0.00343	0.00343	0.04997	0.04997	0.02491	0.02491	0.03335	0.03335
$0.7\sigma_c$	0.00013	0.00356	0.0057	0.05567	0.00632	0.03123	0.00435	0.0377
$0.8\sigma_c$	0.00239	0.00595	0.00394	0.05961	0.00707	0.03831	0.00324	0.04094
$0.9\sigma_c$	0.00168	0.00762	0.00629	0.0659	0.00835	0.04666	0.01404	0.05498
$1.0\sigma_c$	0.01504	0.02266	0.01794	0.08384	0.01696	0.06362	0.94502	1
$1.14/1.17\sigma_c$	0.97734	1	0.91616	1	0.93637	1	/	/

According to the results of damage variables and cumulative damage variables calculated in Table 5, the evolution curves of damage variables and cumulative damage variables

were plotted to describe the change process of rock damage in a more visual way, as shown in Figure 17:

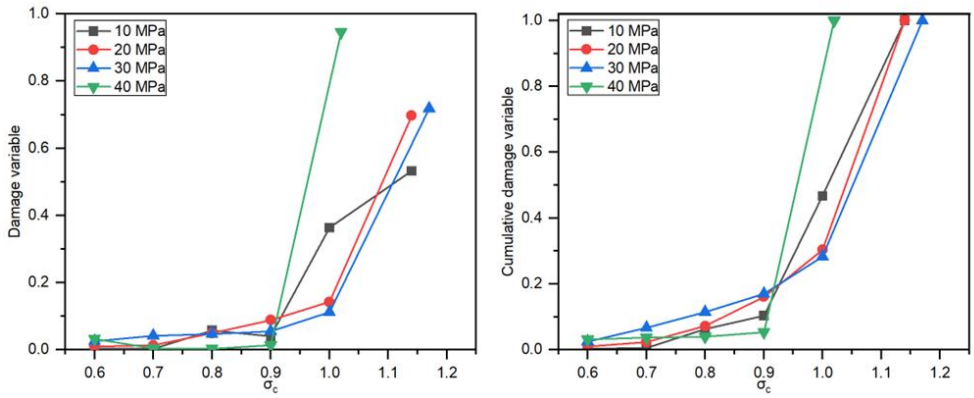

Figure 17. Damage variable curves derived from the characterization of AE counts. (**a**) damage variable versus stress level, (**b**) cumulative damage variable versus stress level.

As shown in Figure 17, the damage variables and cumulative damage variables of the rock specimens generally increased with the increase of the upper stress of the cycles loading, and the damage variables of the specimens under the four confining pressure conditions reached the maximum in the last loading stage. The overall trend shows that the higher the confining pressure, the higher the cumulative damage variable.

In the low stress condition, the rock damage variable is smaller, the cracks develop slowly, and the cumulative damage variable increases at a slower rate. The curves of the specimens with a confining pressure of 10~30 MPa show that both the damage variable and the cumulative damage variable are less than 0.5 when the upper stress is less than or equal to 1.0 σ_c. The curves of the specimens with a confining pressure of 40 MPa show that the damage variable is very small when the upper stress is less than or equal to 0.9 σ_c, the cumulative damage variable is less than 0.06.

In the high stress state, the cracks developed unsteadily, and the rock damage variables increased steeply, and the damage variables all exceeded 0.5 in the last loading stage. The peak stresses of the specimens with an enclosing pressure of 10–30 MPa were enhanced after cyclic loading and unloading, and their peak stresses were 1.14 σ_c, 1.14 σ_c, and 1.17 σ_c, respectively. The specimen's peak strength with a confining pressure of 40 MPa were not increased after cyclic loading. It shows that based on the number of AE events to characterize the rock damage, the rock damage is very small before the peak stress, and the damage exceeding 0.5 is mainly in the unstable development stage of cracks, the rock damage is mainly concentrated in the stage of approaching the peak stress.

4.4. b-Value Analysis in Cyclic Loading–Unloading Tests

In the AE monitoring of rock-like material experiments, the b-value can be used to describe the process of rock crack initiation and expansion evolution to distinguish between macroscopic and microscopic cracks, a high b-value can reflect the generation of microcracks within the rock and slowly expanding [42], and a low b-value reflects the formation of cracks within the rock is fast or unstable, and the value of which is calculated by using the formula as follows [43,44]:

$$\log_{10} N = a - bM_A \tag{13}$$

$$M_A = \frac{A_{dB}}{20} \tag{14}$$

where M_A stands for the AE magnitude; A_{dB} is the peak amplitude of the AE counts; N is the number of AE signals with amplitude greater than A_{dB}; a, b are the fitting parameters, b is the parameter used to characterize the rock crack sprouting and expansion.

According to the AE experimental acquisition frequency, to prevent the results from large errors due to the calculation interval is too small, set every $5A_{dB}$ as a calculation section, combined with the AE monitoring data, the statistical distribution of peak amplitude and its overall accounted for in the cyclic loading experimental under different confining pressures are shown in Figure 18.

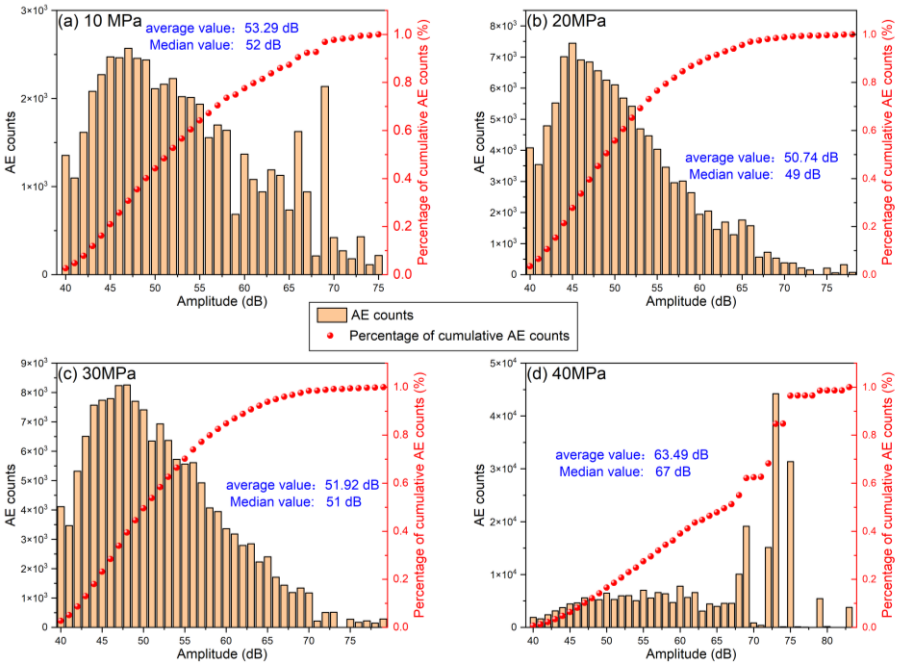

Figure 18. Statistical distribution of AE counts in cycling test. (**a**) 10 MPa confining pressure, (**b**) 20 MPa confining pressure, (**c**) 30 MPa confining pressure, (**d**) 40 MPa confining pressure.

From Figure 18, the AE counts corresponding to each amplitude value roughly show a gradual increase as the confining pressure increases. This indicates that the high confining pressure leads to larger energy release and crack scaling during the cycling process. According to the AE accumulation curves, with the increase of AE amplitude, the AE counts initially showed a linear increase with the increase of the AE amplitude at the perimeter pressure of 10–30 MPa, and then the increase trend was gradually slowed down; at the confining pressure of 40 MPa, there was a jump in the percentage of the accumulated AE counts, the AE amplitude is mainly concentrated in 45~55 dB.

Figure 19 shows the AE b-value and the fitting curves used to determine the b-value, the fitting coefficients are 0.887, 0.957, 0.943, and 0.711, respectively, and the fitting coefficients are higher for the confining pressures of 10–30 MPa, which indicate that the b-values obtained from the AE data are relatively accurate, with b-values of 0.978, 1.380, and 1.296. This shows that for the medium permeability sandstone, the b-value shows an overall increasing trend with the increase of the confining pressure, which indicates that during the loading process, the cracks are formed faster and more unstable under the low perimeter pressure; the fitting coefficient of the perimeter pressure of 40 MPa is general, which indicates that the cracks are non-stable extension under the confining pressure, and the b-value is more difficult to be fitted.

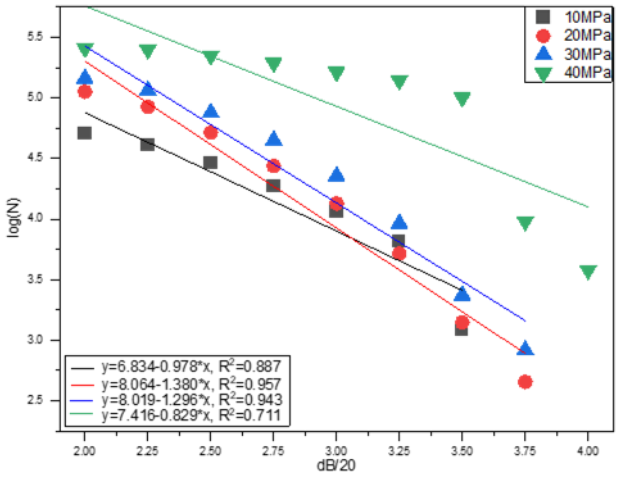

Figure 19. Change in b-value during cyclic loading with linear fitting.

4.5. RAAF Distribution Analysis in Cyclic Loading–Unloading Tests

When shear damage and tensile damage occur, the materials will exhibit different RA (ratio of rise time to amplitude)–AF (ratio of number of impacts to duration) distributions. Rock materials are characterized by high AF and low RA when tensile damage occurs, while low AF and high RA when shear damage occurs [45,46], so the damage pattern of medium permeability sandstones under complex stress conditions can be analyzed by the characteristics of RA–AF distribution. Based on the AE characteristic parameters measured in the experiment, the distribution trend of RA–AF during cyclic loading was analyzed, and the distribution range of RA and AF is shown in Figure 20:

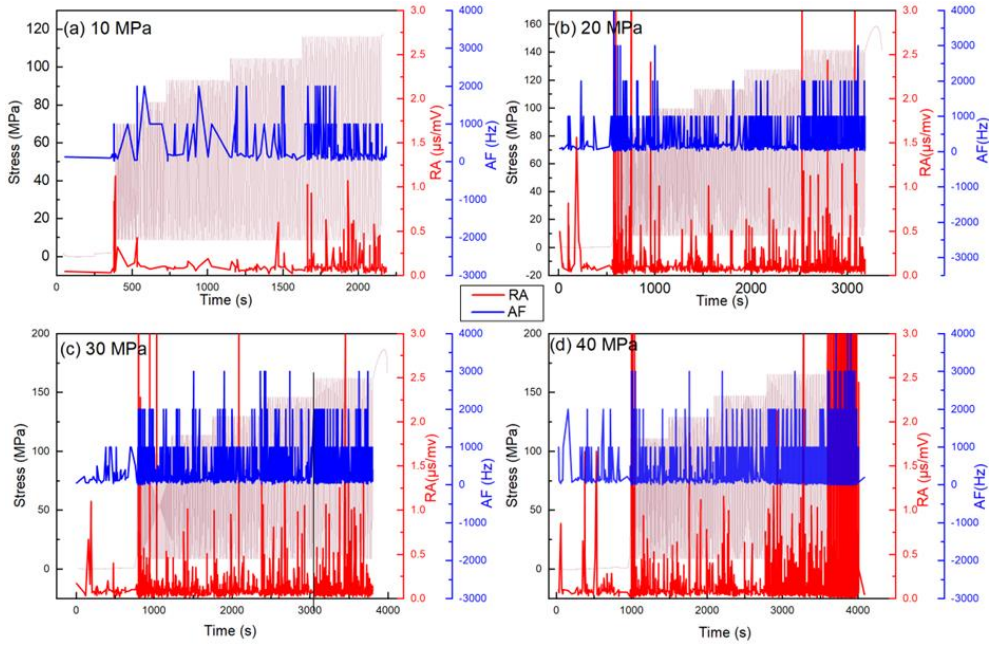

Figure 20. Change curve of RA and AF values during cycling test. (**a**) 10 MPa confining pressure, (**b**) 20 MPa confining pressure, (**c**) 30 MPa confining pressure, (**d**) 40 MPa confining pressure.

As can be seen from Figure 20, the RA and AF values of the samples under different confining pressure conditions show similar trends. At low stress levels, the RA–AF values increase only when the stress level increases, and then the fluctuations gradually stabilize. The RA–AF values gradually increase when the stress level gradually reaches the peak stress of the medium permeability sandstone. This suggests that a sudden increase in stress can lead to significant creation and expansion of cracks in the rock. The AF values increase

slightly at the beginning of each stress level and then fluctuate smoothly. The RA values not only increase significantly at the initial stage of each stress level, but also have multiple jump points with sharp increases several times during the constant amplitude period. This may imply that tensile and small shear cracks are constantly generated in the rock and that shear cracks develop significantly. At high stress levels, the RA–AF values are continuous and intensive, and their values are also relatively large. In addition, the RA–AF values at high confining pressure (40 MPa) are usually larger than those at other confining pressures.

To further study the RA–AF distribution and crack characteristics of the medium-porosity and medium-permeability sandstone during the cyclic loading process, Figure 21 shows the normalized distribution of the original RA–AF data under different confining pressure cyclic loading states. The AF values of the rock samples do not present an intermittent distribution, and the high AF values are relatively sparse; the RA values are not densely distributed along the axial direction, but there are still points with high RA values. This further indicates that the internal damage of the medium-porosity and medium-permeability sandstone under cyclic loading is not of a single type, but a tensile-shear composite type of damage; and the shear type of damage is more obvious when the confining pressure is 10 MPa and 20 MPa.

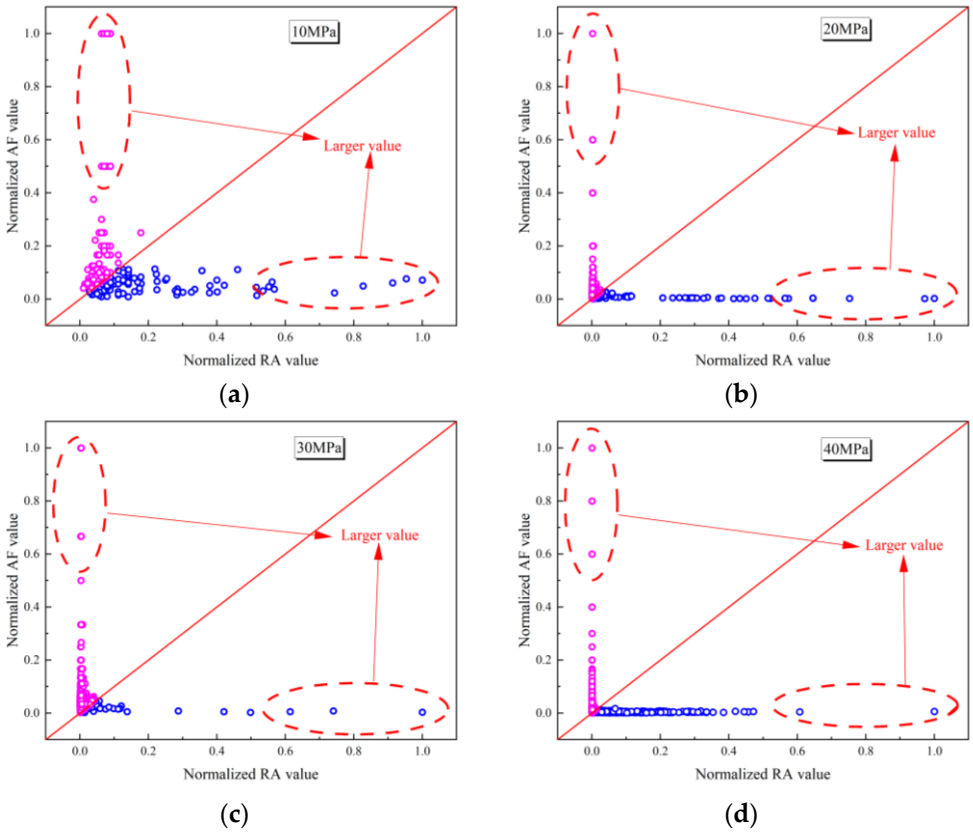

Figure 21. The normalized AF and RA values. (**a**) 10 MPa confining pressure, (**b**) 20 MPa confining pressure, (**c**) 30 MPa confining pressure, (**d**) 40 MPa confining pressure.

5. Conclusions

In this paper, taking sandstone of medium permeability outcrop as the research object, graded cyclic loading triaxial compression experiments were carried out under different confining pressure conditions to analyze the mechanical characteristics and AE characteristics of sandstone samples under different stress levels, and the following main conclusions were obtained:

(1) For sandstone specimens with confining pressures of 10–30 MPa, the peak stresses increased by 14–17% relative to conventional triaxial compression experiments after cyclic loading triaxial compression experiments at five stress levels.

(2) The modulus of elasticity of sandstone increases in general with an increase in the confining pressure. The elastic modulus at the $0.7\sigma_c$ stress level stage showed an obvious overall enhancement relative to the $0.6\sigma_c$ stress level stage, reflecting the predominance of compression densities; the overall elastic model showed different degrees of slow decrease after the $0.8\sigma_c$ stress level stage, the elastic modulus showed a fast decrease, and the rock sample damage was intensified.

(3) The damage variables and cumulative damage variables at different confining pressures increase with an increase in upper stress of the loading cycle. At the last level of loading, the rock damage variable increases very significantly, with an average value of about 0.43 and 0.72, respectively, indicating that the rock damage occurs mainly in the unstable development stage of cracks. Using both methods, it was shown that the rock damage is mainly concentrated near the peak stress stage.

(4) The b value shows an overall increasing trend with an increase in the confining pressure, which indicates that the cracks form faster and more unstable at low confining pressure during the loading process. A sudden increase in stress leads to the emergence and expansion of the cracks in the medium permeability sandstone. Further, it continuously produces tensile and shear type cracks during the cyclic loading process, and the development of the shear cracks is more obvious.

Author Contributions: Writing—original draft, D.X.; Investigation, D.X.; Project administration, H.L. (Hejuan Liu); Writing—review and editing, H.L. (Hejuan Liu) and J.L. (Jianjun Liu); Methodology, D.X. and Y.G.; Formal analysis, Y.G., J.L. (Jun Lu) and M.L.; Data curation, X.Q., H.L. (Haibo Li) and H.T.; Visualization, J.L. (Jun Lu), H.L. (Haibo Li) and M.L.; Funding acquisition, D.X. and H.L (Hejuan Liu). All authors have read and agreed to the published version of the manuscript.

Funding: This research was funded by the Young Scientists Fund of the National Natural Science Foundation of China (No. 52204076), Open Foundation of China National Petroleum Corporation Science and Technology Research Institute Limited (RIPED.CN-2023-JS-580), Open Research Fund of State Key Laboratory of Geo-mechanics and Geotechnical Engineering, Institute of Rock and Soil Mechanics, Chinese Academy of Sciences, Grant NO SKLGME022020.

Data Availability Statement: The data to support the findings of this study are available from the corresponding author upon request.

Conflicts of Interest: Authors Mancang Liu and Xiaosong Qiu were employed by the company China National Petroleum Corporation. Author Haibo Li was employed by the company PetroChina Company Limited. The remaining authors declare that the research was conducted in the absence of any commercial or financial relationships that could be construed as a potential conflict of interest.

References

1. Al-Shafi, M.; Massarweh, O.; Abushaikha, A.S.; Bicer, Y. A review on underground gas storage systems: Natural gas, hydrogen and carbon sequestration. *Energy Rep.* **2023**, *9*, 6251–6266.
2. Liu, H.; Yang, C.; Liu, J.; Hou, Z.; Xie, Y.; Shi, X. An overview of underground energy storage in porous media and development in China. *Gas Sci. Eng.* **2023**, *117*, 205079.
3. Zhou, Y.; Sheng, Q.; Li, N.; Fu, X. The relationship between dynamic strength and strain rate and damage to rock materials subjected to dynamic cyclic loading. *Geomech. Geophys. Geo-Energy Geo-Resour.* **2021**, *7*, 88.
4. Hu, M.; Xu, W.; Wang, H.; Ning, Y.; Wang, R.; Lyu, C.; Zhang, T. Deformation characteristics of muddy sandstones during cyclic loading and unloading with different stress lower limits under pore pressure. *Int. J. Fatigue* **2023**, *172*, 107606.
5. Wang, M.; Li, J.; Tan, H.; Wang, J.; Shi, Z.; Li, K. Study on fatigue characteristics and thermal damage mechanism of red sandstone under high temperature-cyclic load coupling. *Int. J. Fatigue* **2023**, *168*, 107405.
6. Wang, S.; Xu, W.; Sun, M.; Wang, W. Experimental investigation of the mechanical properties of fine-grained sandstone in the triaxial cyclic loading test. *Environ. Earth Sci.* **2019**, *78*, 416.
7. Zhou, J.; Deng, G.; Tian, S.; Xian, X.; Yang, K.; Zhang, C.; Dong, Z. Experimental study on the permeability variation of sandstone at cyclic stress: Implication for underground gas storage. *J. Energy Storage* **2023**, *60*, 106677.
8. Shirani Faradonbeh, R.; Taheri, A.; Karakus, M. Post-peak behaviour of rocks under cyclic loading using a double-criteria damage-controlled test method. *Bull. Eng. Geol. Environ.* **2021**, *80*, 1713–1727.
9. Shirani Faradonbeh, R.; Taheri, A.; Karakus, M. Failure Behaviour of a Sandstone Subjected to the Systematic Cyclic Loading: Insights from the Double-Criteria Damage-Controlled Test Method. *Rock Mech. Rock Eng.* **2021**, *54*, 5555–5575.

10. You, W.; Dai, F.; Liu, Y.; Yan, Z. Effect of confining pressure and strain rate on mechanical behaviors and failure characteristics of sandstone containing a pre-existing flaw. *Rock Mech. Rock Eng.* **2022**, *55*, 2091–2109.
11. Yang, D.; Hu, J.; Ding, X. Analysis of energy dissipation characteristics in granite under high confining pressure cyclic load. *Alex. Eng. J.* **2020**, *59*, 3587–3597.
12. Kang, P.; Jiaqi, Z.; Quanle, Z.; Junhui, M. Fatigue deformation characteristics and damage model of sandstones subjected to cyclic loading: Implications for fatigue life prediction. *Int. J. Geomech.* **2022**, *22*, 04021261.
13. Geranmayeh Vaneghi, R.; Thoeni, K.; Dyskin, A.V.; Sharifzadeh, M.; Sarmadivaleh, M. Strength and damage response of sandstone and granodiorite under different loading conditions of multistage uniaxial cyclic compression. *Int. J. Geomech.* **2020**, *20*, 04020159.
14. Munoz, H.; Taheri, A. Postpeak Deformability Parameters of Localized and Nonlocalized Damage Zones of Rocks under Cyclic Loading. *Geotech. Test. J.* **2019**, *42*, 1663–1684.
15. Zhu, X.; Li, Y.; Wang, C.; Sun, X.; Liu, Z. Deformation failure characteristics and loading rate effect of sandstone under uniaxial cyclic loading and unloading. *Geotech. Geol. Eng.* **2019**, *37*, 1147–1154.
16. Liu, Y.; Dai, F. A review of experimental and theoretical research on the deformation and failure behavior of rocks subjected to cyclic loading. *J. Rock Mech. Geotech. Eng.* **2021**, *13*, 1203–1230.
17. Peng, K.; Wang, Y.; Zou, Q.; Cheng, Y.; Song, X. Experimental study of energy dissipation characteristics and crack coalescence modes of cracked sandstone under different cyclic loading paths. *Bull. Eng. Geol. Environ.* **2021**, *80*, 5881–5895.
18. Šancer, J.; Štrejbar, M.; Maleňáková, A. Effects of cyclic loading on the rheological properties of sandstones. *Cent. Eur. J. Geosci.* **2011**, *3*, 207–214.
19. Peng, K.; Zhou, J.; Zou, Q.; Zhang, Y.; Tan, G. Deformation characteristics and failure modes of sandstones under discontinuous multi-level cyclic loads. *Powder Technol.* **2020**, *373*, 599–613.
20. Yu, X.; Tan, Y.; Song, W.; Kemeny, J.; Qi, S.; Zheng, B.; Guo, S.-f. Damage evolution of rock-encased-backfill structure under stepwise cyclic triaxial loading. *J. Rock Mech. Geotech. Eng.* **2024**, *16*, 597–615.
21. Deng, G.; Zhou, J.; Tian, S.; Xian, X.; Zhou, L.; Zhang, C.; Li, S.; Tan, Y. Pore structure changes and its stress-sensitive behavior in sandstone under cyclic stress: Implication for underground gas storage. *Gas Sci. Eng.* **2023**, *119*, 205130.
22. Duan, X.-l.; Wang, W.; Liu, S.-f.; Cao, Y.; Zheng, Z.; Zhu, Q. Experimental investigation on mechanical behavior, energy evolution and gas permeability of anisotropic phyllite subjected to triaxial compression and cyclic loading. *Geomech. Energy Environ.* **2023**, *35*, 100483.
23. Hu, K.; Fu, H.; Li, J.; Deng, H. Constitutive model for simulating the mechanical behaviour of rock under triaxial cyclic loading. *Comput. Geotech.* **2023**, *159*, 105420.
24. Wang, J.; Li, J.; Shi, Z.Y.; Chen, J.; Lin, H. Fatigue characteristics and fracture behaviour of sandstone under discontinuous multilevel constant-amplitude fatigue disturbance. *Eng. Fract. Mech.* **2022**, *274*, 108773.
25. Zhang, T.; Xu, W.; Wang, R.; Yan, L.; He, M. Deformation characteristics of cement mortar under triaxial cyclic loading: An experimental investigation. *Int. J. Fatigue* **2021**, *150*, 106305.
26. Shen, R.; Chen, T.; Li, T.; Li, H.; Fan, W.; Hou, Z.; Zhang, X. Study on the effect of the lower limit of cyclic stress on the mechanical properties and acoustic emission of sandstone under cyclic loading and unloading. *Theor. Appl. Fract. Mech.* **2020**, *108*, 102661.
27. Wang, Y.; Gao, S.H.; Li, C.H.; Han, J.Q. Energy dissipation and damage evolution for dynamic fracture of marble subjected to freeze-thaw and multiple level compressive fatigue loading. *Int. J. Fatigue* **2021**, *142*, 105927.
28. Du, K.; Li, X.; Tao, M.; Wang, S. Experimental study on acoustic emission (AE) characteristics and crack classification during rock fracture in several basic lab tests. *Int. J. Rock Mech. Min. Sci.* **2020**, *133*, 104411.
29. Gao, Y.; Lan, D.; Yang, S.; Hou, P.; Wang, Y.; Ding, F. The Acoustic Emission Behavior and Its Fractal Characteristics of the Sandstone Under the Disturbance Stress Paths. *Rock Mech. Rock Eng.* **2023**, *56*, 5487–5511.
30. Zhang, H.; Guo, J.; Sun, F.; Shi, X.; Zhu, Z. Experimental Study on Acoustic Emission Characteristics in the Fracture Process of Granite Under Dry and Saturated State. *Geotech. Geol. Eng.* **2022**, *40*, 5213–5231.
31. Li, D.; Wang, E.; Kong, X.; Ali, M.; Wang, D. Mechanical behaviors and acoustic emission fractal characteristics of coal specimens with a pre-existing flaw of various inclinations under uniaxial compression. *Int. J. Rock Mech. Min. Sci.* **2019**, *116*, 38–51.
32. Li, H.; Ma, H.; Yang, C.; Zhao, K.; Hu, Z.; Daemen, J. Acoustic emission characteristics of rock salt under multi-stage cyclic loading. *Int. J. Fatigue* **2023**, *176*, 107911.
33. Tang, C.A.; Chen, Z.H.; Xu, X.H.; Li, C. A Theoretical Model for Kaiser Effect in Rock. *Pure Appl. Geophys.* **1997**, *150*, 203–215.
34. Zhao, K.; Ma, H.; Yang, C.; Daemen, J.J.K. The role of prior creep duration on the acoustic emission characteristics of rock salt under cyclic loading. *Int. J. Rock Mech. Min. Sci.* **2022**, *157*, 105166.
35. Li, Z.; Suo, J.; Fan, J.; Fourmeau, M.; Jiang, D.; Nelias, D. Damage evolution of rock salt under multilevel amplitude creep–fatigue loading with acoustic emission monitoring. *Int. J. Rock Mech. Min. Sci.* **2023**, *164*, 105346.
36. Zhang, L.; Cong, Y.; Meng, F.; Wang, Z.; Zhang, P.; Gao, S. Energy evolution analysis and failure criteria for rock under different stress paths. *Acta Geotech.* **2021**, *16*, 569–580.
37. Li, T.; Pei, X.; Wang, D.; Huang, R.; Tang, H. Nonlinear behavior and damage model for fractured rock under cyclic loading based on energy dissipation principle. *Eng. Fract. Mech.* **2019**, *206*, 330–341.
38. Gao, Y.; Feng, X.-T. Study on damage evolution of intact and jointed marble subjected to cyclic true triaxial loading. *Eng. Fract. Mech.* **2019**, *215*, 224–234.

39. Chen, Z.; He, C.; Ma, G.; Xu, G.; Ma, C. Energy Damage Evolution Mechanism of Rock and Its Application to Brittleness Evaluation. *Rock Mech. Rock Eng.* **2019**, *52*, 1265–1274.
40. Peng, R.; Xie, H.; Ju, Y.; Zhou, H. Influence of elastic energy storage in testing machines on the testing of mechanical properties of rocks. *Mech. Eng.* **2005**, 51–55.
41. Chen, Z.; Tang, C.; Xu, X.; Li, C. Theoretical and experimental study of the Kaiser effect in rock acoustic emission. *Chin. J. Nonferrous Met.* **1997**, 12–15.
42. Liu, M.; Lu, J.; Ming, P.; Song, J. AE-based damage identification of concrete structures under monotonic and fatigue loading. *Constr. Build. Mater.* **2023**, *377*, 131112.
43. Shi, Z.; Li, J.; Wang, J. Effect of creep load on fatigue behavior and acoustic emission characteristics of sandstone containing pre-existing crack during fatigue loading. *Theor. Appl. Fract. Mech.* **2022**, *119*, 103296.
44. Li, S.; Yang, D.; Huang, Z.; Gu, Q.; Zhao, K. Acoustic emission characteristics and failure mode analysis of rock failure under complex stress state. *Theor. Appl. Fract. Mech.* **2022**, *122*, 103666.
45. Dong, L.; Zhang, Y.; Bi, S.; Ma, J.; Yan, Y.; Cao, H. Uncertainty investigation for the classification of rock micro-fracture types using acoustic emission parameters. *Int. J. Rock Mech. Min. Sci.* **2023**, *162*, 105292.
46. Zhao, K.; Yang, D.; Gong, C.; Zhuo, Y.; Wang, X.; Zhong, W. Evaluation of internal microcrack evolution in red sandstone based on time–frequency domain characteristics of acoustic emission signals. *Constr. Build. Mater.* **2020**, *260*, 120435.